Materials Advances

ROYAL SOCIETY OF CHEMISTRY

PAPER

View Article Online
View Journal | View Issue

Cite this: *Mater. Adv.*, 2025, 6, 4389

A naphthalimide-derived chemosensor for ratiometric detection of sulphide ions: insights into the S^{2-}-driven reduction cascade, real-time applications and live cell imaging of bacterial cells†

Saurabh Gupta,[ab] Gulshan Kumar,[c] Vijay Luxami[a] and Kamaldeep Paul*[ab]

Hydrogen sulphide (H_2S) is an unpleasant, harmful gas commonly found in the environment, released from geothermal vents, and produced as a byproduct in industries such as oil refining and wastewater treatment. Because of its extreme toxicity, there is growing concern about its presence, necessitating timely detection to ensure human welfare. However, detecting H_2S in various environments, including air and water, remains a significant challenge. To develop a probe for sulphide ion detection, herein, we report the synthesis of a highly selective, sensitive, and colorimetric chemosensor (**NATRP**) for the detection of sulphide ions (S^{2-}) in a 50% aqueous medium. **NATRP** demonstrates exceptional sensitivity and selectivity for S^{2-} ions relative to other ions, with a limit of quantification of 26 nM and a detection limit of 7.9 nM. It shows aggregation-induced emission quenching, which upon the addition of S^{2-} ions, disaggregates with enhancement in fluorescence intensity. This enables **NATRP** to detect S^{2-} ions within 15 seconds and it demonstrates good pH stability, suggesting that **NATRP** can detect sulphide ions across a broad pH range. The mechanism underlying the detection involves the reduction of azide groups to amine groups in the presence of S^{2-} ions, confirmed by NMR titrations and HRMS analysis. Furthermore, **NATRP** successfully detects S^{2-} ions in water, serum and solid samples, as well as in live cell imaging in bacterial cells. Moreover, UV-visible and fluorescence data have been employed to construct 1-to-2 decoders.

Received 6th February 2025,
Accepted 13th May 2025

DOI: 10.1039/d5ma00103j

rsc.li/materials-advances

1. Introduction

Sulphide ions (S^{2-}) are highly toxic and cause various health issues, including respiratory system failure. They are mostly derived from the growth of the petrochemical and leather manufacturing industries, as well as human metabolism.[1,2] Both protonated (HS^- and H_2S) and non-protonated (S^{2-} ions) species are hazardous, which makes the situation worse, due to their presence in the environment and wastewater in certain quantities.[3] Exposure to water contaminated with S^{2-} ions, which dissociate into HS^- and H_2S, has been linked to diseases such as Alzheimer's, liver cirrhosis, and Down's syndrome.[4,5] Hydrogen sulphide (H_2S) is involved in various critical physiological processes, including inflammation, angiogenesis, neuromodulation, *etc.*, and it has drawn interest as an essential endogenous gasotransmitter.[6,7] In addition, it plays a vital role in the biological system and is extensively distributed throughout various organs, including the brain, spleen, liver, and heart.[8] This underscores the importance of regulating sulfide discharge and adhering to environmental protection guidelines. However, accurate and efficient detection of S^{2-} ions in aqueous environments and living systems has become an urgent necessity.[9,10] A number of techniques for detecting S^{2-} ions have been ascribed, including ion chromatography, colorimetric, electrochemical methods, and inductively coupled plasma atomic emission spectroscopy.[11] These conventional techniques have a number of inherent shortcomings, such as operation complexity, limited sensitivity, and poor precision, which limit their use for quick and precise detection of S^{2-} ions, especially in biological systems.[12,13] Addressing these challenges requires innovative, user-friendly, and efficient detection methods capable of tracking S^{2-} ions in complex and dynamic physiological environments.[14] In recent years, the fluorogenic probes have gained significant attention because of

[a] *Department of Chemistry and Biochemistry, Thapar Institute of Engineering and Technology, Patiala, 147004, India. E-mail: kpaul@thapar.edu*
[b] *TIET-VT, Centre of Excellence in Emerging Materials, Thapar Institute of Engineering and Technology, Patiala, Punjab, India 147004*
[c] *Department of Chemistry, Banasthali University, Banasthali Newai, 304022, Rajasthan, India*

† Electronic supplementary information (ESI) available. See DOI: https://doi.org/10.1039/d5ma00103j

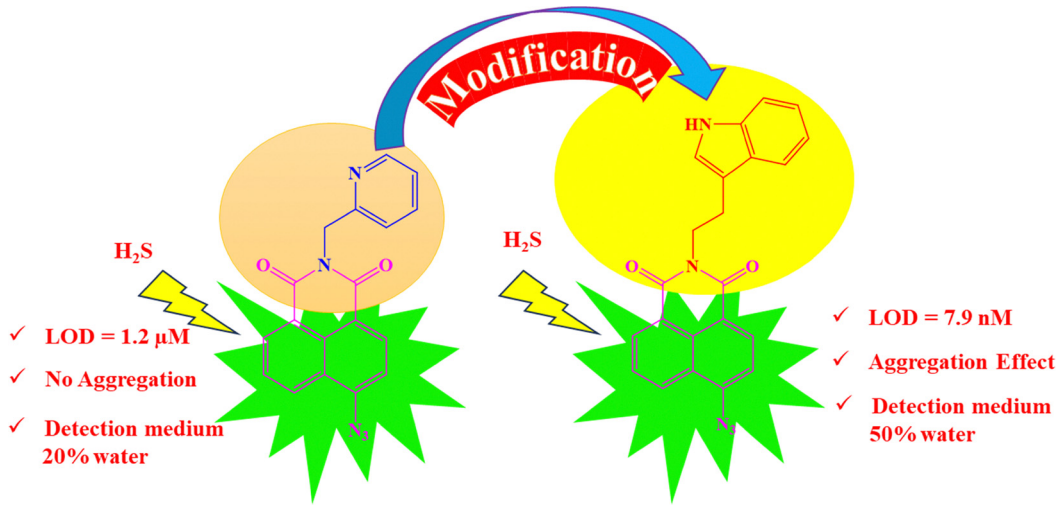

Fig. 1 Design of probe **NATRP**.

their non-invasive nature, ease of use, high selectivity, amazing fluorescence changes, and real-time imaging capabilities that can also be applied to living cells, and organisms.[15,16] While several fluorescent probes for S^{2-} detection have been reported, their design strategies typically rely on the reactive characteristics of S^{2-} ions, such as amide-iminol tautomerism, nitro and azide reduction, H_2S-mediated hydroxyl amide reactions, copper-sulfide precipitation, spiro-lactam ring opening, and dual nucleophilic addition.[17–19] The development of innovative S^{2-} ion probes is still important because of the intricacy of the molecular activities involved in signaling transduction and other issues connected to the probes.[20] Recently, fluorescent probes and transition metal complexes have been specifically produced for the detection of H_2S in aqueous media using a coordination approach. Organic azide-based chemosensors have also been explored,[21] but challenges such as synthetic complexity, reliance on organic solvents, interference from other biothiols, and limited biological imaging capabilities remain to be addressed.[22] Naphthalimide-based sensor systems have emerged as promising tools for H_2S detection, offering several advantages, including a simple single-step reaction, good yield, high sensitivity and selectivity, low cost, rapid response, and non-destructive nature.[23] These attributes make naphthalimide-based sensors an appealing solution for detecting sulfide ions in diverse applications.

1.1 Design of the NATRP

Over the past few years, naphthalimide-based fluorescent probes have been extensively developed for the detection of H_2S, utilizing the azide group as the primary site for sensing (Table S1, ESI†). However, these sensors often exhibit limitations, including detection limits in the micromolar (μM) range and slow response times, which hinder their practical applicability for rapid and efficient H_2S detection across diverse sample types. In 2022, Jothi *et al.* developed a naphthalimide-based fluorescent matrix for detecting H_2S with the pyridyl group at an anhydride position.[6] This probe detected H_2S in a 20% water medium with a detection limit of 1.2 μM. To address the above issues, we modified the probe, replacing the pyridyl group with tryptamine. Tryptamine is known to regulate gastrointestinal motility by activating 5-HT4 receptors in the human gut, which may aid in the specific detection of sulphide ions. The synthesized probe demonstrated remarkable selectivity and sensitivity, detecting S^{2-} ions in a 50% aqueous medium with a detection limit in the nanomolar (nM) range. Additionally, the synthesized compound exhibited aggregation-induced emission quenching, which was reversed upon interaction with S^{2-} ions, resulting in "turn-on" fluorescence. This feature not only enhances sensitivity but also provides a reliable fluorescence-based tool for selective recognition of S^{2-} ions. The probe proved effective in detecting sulfide ions in water, serum, and solid samples, as well as in live cell imaging in bacterial cells, establishing it as a versatile and efficient solution for real-world applications (Fig. 1).

2. Experimental section

2.1 Synthesis of 2-(2-(1*H*-indol-3-yl)ethyl)-6-azido-1*H*-benzo[*de*]isoquinoline-1,3(2*H*)-dione (NATRP)

To a stirred solution of compound **4** (0.5 g, 2.09 mmol) in ethanol (30 mL), tryptamine (0.33 g, 2.09 mmol) was added in the presence of zinc acetate (0.038 g, 0.16 mmol), and the reaction mixture was refluxed for 8 h. The reaction was monitored with the help of TLC, and on completion of the reaction, 100 mL cold water was added resulting in the formation of dark yellow precipitates, which were filtered and vacuum-dried to obtain the crude product. The product was purified by column chromatography using chloroform and ethyl acetate (8 : 2) as eluents to get the pure brownish-yellow product with 83% yield. The formation of compound **NATRP** was confirmed by the NMR spectroscopy technique (Fig. S1 and S2, ESI†). ^{1}H NMR (400 MHz, $CDCl_3$ + DMSO-d_6): δ 8.50 (dd, ^2J = 11.9, ^3J = 7.5 Hz, 2H, ArH), 8.38 (d, J = 7.7 Hz, 1H, ArH), 7.79–7.73 (m, 1H, ArH), 7.70 (d, J = 7.7 Hz, 1H, ArH), 7.60 (d, J = 8.0 Hz, 1H, ArH), 7.27 (d, J = 7.9 Hz, 1H, ArH), 7.09 (d, J = 2.0 Hz, 1H, ArH), 7.00 (t, J = 7.1 Hz, 1H, ArH), 6.94 (t, J = 7.2 Hz, 1H, ArH), 4.31–4.23

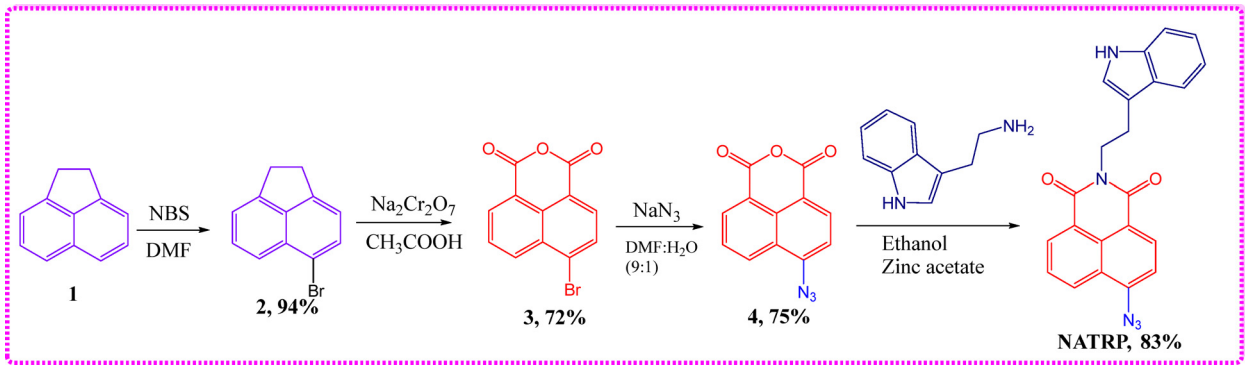

Scheme 1 Synthetic route for the synthesis of **NATRP**.

(m, 2H, CH_2), 3.04–2.95 (m, 2H, CH_2); ^{13}C NMR (DMSO-d_6, 100 MHz): δ (ppm) 162.3, 161.8, 142.0, 135.3, 130.6, 130.4, 127.5, 126.2, 125.8, 122.9, 121.5, 120.0, 117.4, 114.1, 110.3, 28.2, 22.8; HRMS (ESI) calcd for $C_{27}H_{22}N_8O_3$ $[M + H]^+$ 382.1297 found; 382.1299 (Scheme 1).

2.2 Detection of Na_2S in real samples

To detect S^{2-} ions for real time applications, the water samples were collected from different sources like Ganga river water (Haridwar), Ghaggar river water (Ambala), and tap water (from the laboratory). The quantitative applications of S^{2-} ions were estimated through a calibration curve. All these samples were further spiked with different concentrations of S^{2-} ions (10, 20, 30, 40 μM). **NATRP** (20 μM) was added to these solutions (3 mL) having different S^{2-} ion concentrations. The spiked samples were estimated over the calibration curve.

3. Results and discussion

3.1 Photophysical behaviour of NATRP

Additional measurements of steady-state absorption and emission spectra were observed in a variety of solvents. It was found that the absorption maxima lie between 344 and 378 nm and the emission maxima exist between 435 and 530 nm, in different solvent systems (Fig. S3, ESI†). These redshifts in the absorption and emission spectra suggested the occurrence of intramolecular charge transfer (ICT). These findings were also corroborated with subsequent computational calculations, which showed shifting of electron density from tryptamine to the naphthalimide unit.

3.2 Aggregation studies

Aggregation studies were conducted by recording absorption and emission spectra in CH_3CN with progressive addition of H_2O in order to check the aggregation behaviour of the synthesized compound. The solution of **NATRP** (20 μM, CH_3CN) exhibited an absorption band at 370 nm. With gradual addition of water from 0 to 40%, a slight increase and a shift in absorption maxima were observed. With a further increase in water ratio from 50 to 100%, a decrease in absorption maximum was recorded with a levelling off at 750 nm, indicative of the formation of aggregates in the medium (Fig. 2a). Emission studies were also performed to confirm aggregation in the solution of **NATRP**, which exhibited an intense emission band at 530 nm in CH_3CN with a quantum yield (Φ_f) of 0.45. With progressive addition of water in solution, a constant decrease in emission intensity of **NATRP** was observed with a decrease in quantum yield to 0.27 in $CH_3CN : H_2O$ (1 : 1); and in pure water, the emission intensity of the compound was quenched entirely with a quantum yield (Φ_f) of 0.10, indicating the existence of aggregation-induced emission quenching (Fig. 2b).

A dynamic light scattering (DLS) experiment was performed to examine the effect of increasing water concentration on the particle size of **NATRP**, which also confirmed the aggregation behaviour of the compound. In pure CH_3CN, **NATRP** exhibited an average particle size of 133 nm with a PDI value of 0.262. On increasing the water ratio in CH_3CN, the average hydrodynamic size of **NATRP** was increased. In 50% H_2O/CH_3CN, the average particle size was found to be 226 nm having a PDI value of 0.347, and in 90% H_2O/CH_3CN, the particle size was increased to 269 nm with a PDI value of 0.363, indicating the formation of aggregates, and the increase in PDI value assisted the homogeneity of the particles with an increase in H_2O. The maximum change in particle size of approximately 100 nm was recorded from pure CH_3CN to 50% H_2O/CH_3CN ratio; afterwards, no such significant change in the size of the particles was observed and only a change of 40 nm was recorded from 50% to 90% H_2O/CH_3CN ratio. Furthermore, upon addition of S^{2-} to the solution of **NATRP** in 50% H_2O/CH_3CN, the average particle size of a molecule was recorded to be 142 nm with a PDI value of 0.753, implying the disaggregation of the formed aggregates and resulting in homogeneity of the solution (Fig. 2c).

Furthermore, FE-SEM images of **NATRP** were recorded to check the morphological changes in the structure upon increasing the water concentration. **NATRP** exhibited a circular shape morphology in pure CH_3CN. In contrast, upon increase in the water concentration to 50%, the compound exhibited needle-like structures. With a further increase to 80% water, a long needle-like structure was observed. In contrast, in 90% water, the particle size increased, showing more random structures whereas in pure H_2O, the compound exhibited needles as well as rod-like morphologies (Fig. 3a–e). This change in the morphology of the structure confirmed the formation of aggregates. Furthermore, with addition of S^{2-} ions to the solution of

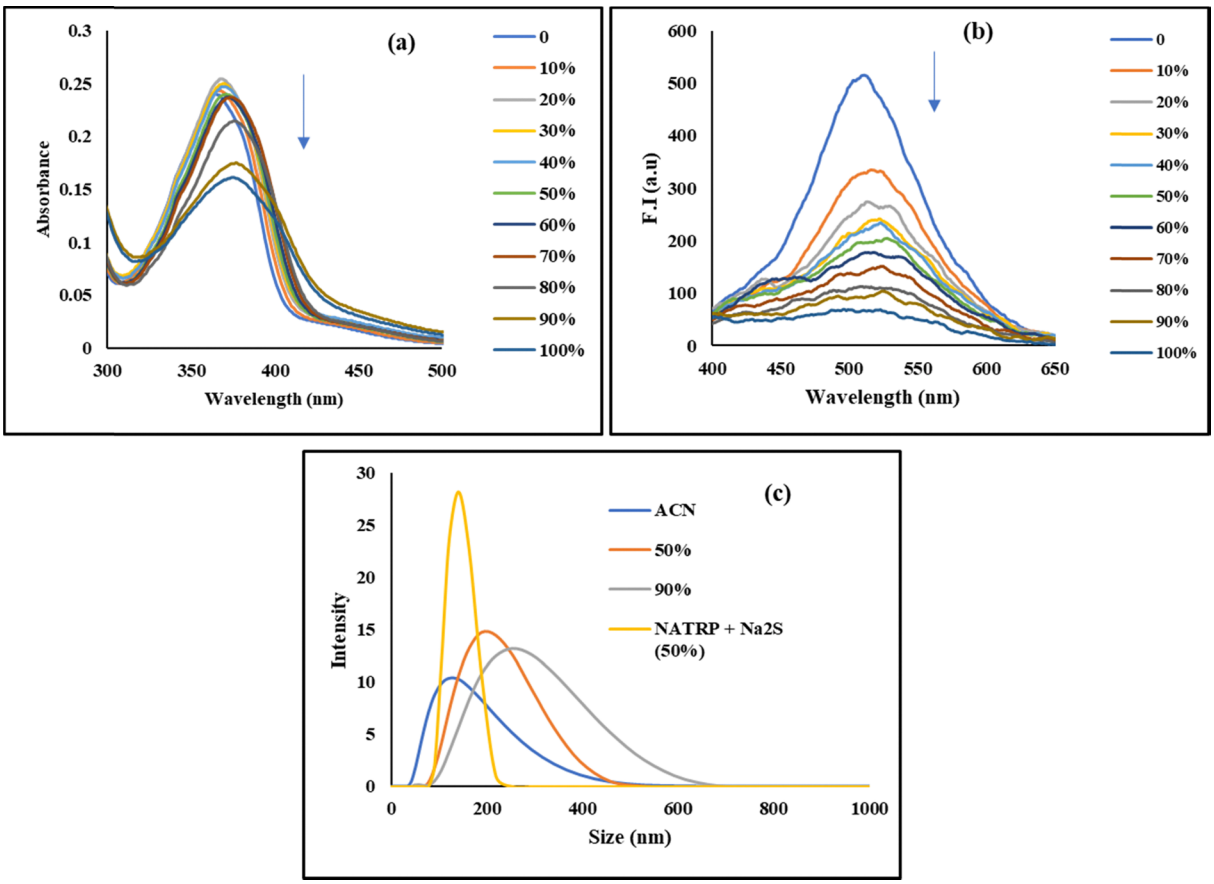

Fig. 2 (a) Absorption and (b) emission spectra of **NATRP** (20 μM) with incremental addition of H_2O in CH_3CN; (c) hydrodynamic size of **NATRP** in CH_3CN, in varying concentrations of CH_3CN:H_2O and in the presence of S^{2-} ions.

NATRP in 50% H_2O/CH_3CN, the compound displayed a cubical shape morphology (Fig. 3f). This might be due to the reduction of the azide group into an amine upon the addition of sulfide ions. Furthermore, the size of a particle of **NATRP** in pure

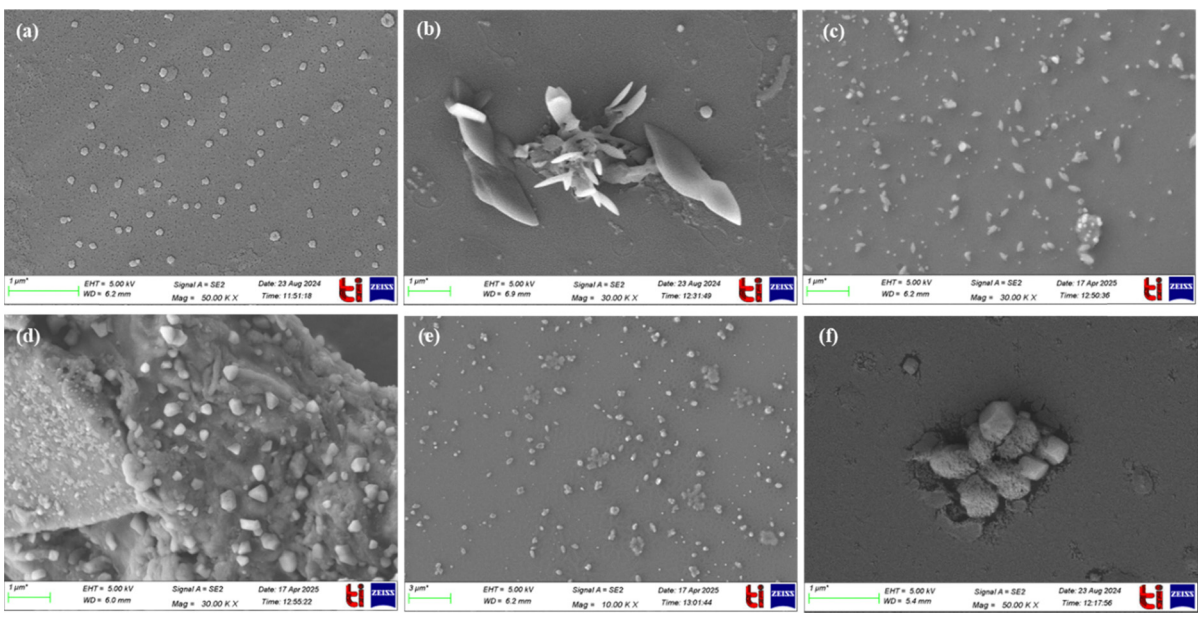

Fig. 3 FE-SEM images of **NATRP** in (a) CH_3CN; (b) 50% (H_2O:CH_3CN); (c) 80% (H_2O:CH_3CN); (d) 90% (H_2O:CH_3CN); (e) H_2O; (f) the presence of S^{2-} ions in 50% H_2O:CH_3CN.

Table 1 Fluorescence lifetime measurements of **NATRP** with increasing concentration of water

	τ_1 (ns)	τ_2 (ns)	α_1	α_2	τ_{av} (ns)	χ^2
CH_3CN	1.86	7.52	0.53	0.47	4.52	1.10
$CH_3CN:H_2O$ (8:2)	1.77	6.32	0.59	0.41	3.63	0.97
$CH_3CN:H_2O$ (1:1)	1.66	6.46	0.72	0.28	2.98	1.10
$CH_3CN:H_2O$ (2:8)	1.54	5.80	0.74	0.26	2.67	1.12
H_2O	1.60	6.77	0.80	0.2	2.63	1.10

CH_3CN was found to be 163.2 nm and in 50% H_2O:CH_3CN, aggregates were formed with a particle size of 230 nm, while upon addition of S^{2-} ions, the particle size was reduced to 150 nm. Thus, both the FE-SEM and DLS results were in coherence.

In addition to this, we further explored the aggregation-induced emission quenching behaviour of **NATRP** upon increasing the water concentration by performing time-correlated single photon counting studies. We recorded the average lifetime of **NATRP** in CH_3CN and with increasing water concentration. In CH_3CN, **NATRP** exhibited an average lifetime of 4.52 ns with two decay components having lifetime values of 1.86 ns and 7.52 ns, with populations of 53% and 47% (Table 1). On increasing the water concentration, *i.e.*, $CH_3CN:H_2O$ (8:2), a drop in lifetime of **NATRP** from 4.52 ns to 3.63 ns was observed, having two decay components with lifetime values of 1.77 ns and 6.32 ns and populations of 59% and 41%. Further increasing the water content to 50%, *i.e.*, $CH_3CN:H_2O$ (1:1), a significant decrease in average lifetime of **NATRP** was recorded, and the lifetime was reduced to 2.98 ns with decay components having lifetime values and populations of 1.66 ns, 6.46 ns and 72%, 26%, respectively. On further increasing the water content, *i.e.* $CH_3CN:H_2O$ (2:8), no significant change in the average lifetime of **NATRP** was observed compared to the average lifetime of **NATRP** in $CH_3CN:H_2O$ (1:1). The average lifetime of **NATRP** in $CH_3CN:H_2O$ (2:8) was found to be 2.67 ns with two decay components having lifetime values of 1.54 ns and 5.80 ns, with populations of 74% and 26%. Meanwhile, in water, the average lifetime of **NATRP** was found to be 2.63 ns, with two decay components having lifetime values of 1.60 ns and 6.77 ns, with populations of 80% and 20%. The decrease in average lifetime of **NATRP** with increasing water concentration may be due to the formation of aggregates, which causes quenching; therefore, the lifetime decreases. The results obtained from time-resolved studies were in accordance with the results obtained from steady-state fluorescence, DLS, and SEM studies.

Summing up the above studies conducted to understand the aggregation behaviour of **NATRP** with increasing concentration of water, it is observed that maximum aggregates of **NATRP** are formed up to 50% $CH_3CN:H_2O$ (1:1) with a significant decrease in lifetime of **NATRP**. Further increasing the water concentration, little change in the particle size or lifetime of **NATRP** was observed, indicating that maximum changes are achieved until 50% $CH_3CN:H_2O$ (1:1); after that, less changes are seen due to quenching in the emission intensity of **NATRP**.

3.3 Sensing properties of NATRP

3.3.1 UV-visible response of NATRP towards anions. The UV-visible spectroscopy technique was employed to determine the sensing properties of **NATRP** towards various anions. Initially, the ability of **NATRP** to detect analytes was conducted in different solvents like CH_3CN, CH_3OH, H_2O, CH_3CN/H_2O, and CH_3OH/H_2O. Promising results were obtained in $CH_3CN:H_2O$ (1:1), where the maximum sensitivity and selectivity have

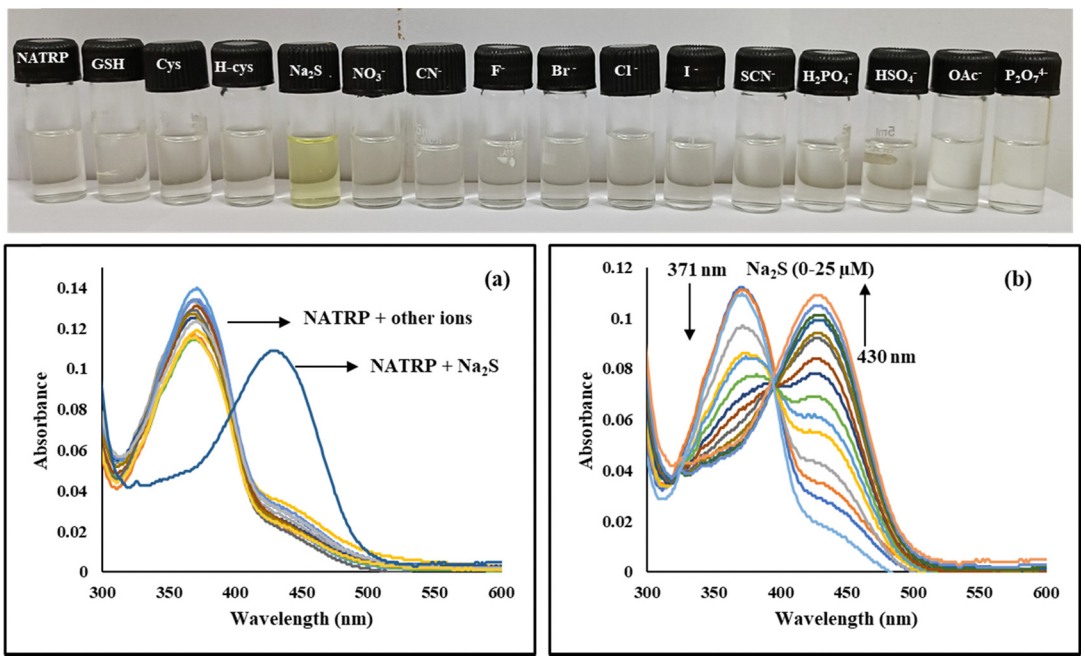

Fig. 4 UV-visible spectra of **NATRP** (20 μM) in a $CH_3CN:H_2O$ ratio (1:1, [v/v], pH = 7.3); (a) in the presence of various anions and (b) upon increasing concentration (0–25 μM) of S^{2-}ions; Inset: Visible color change of **NATRP** after adding different anions.

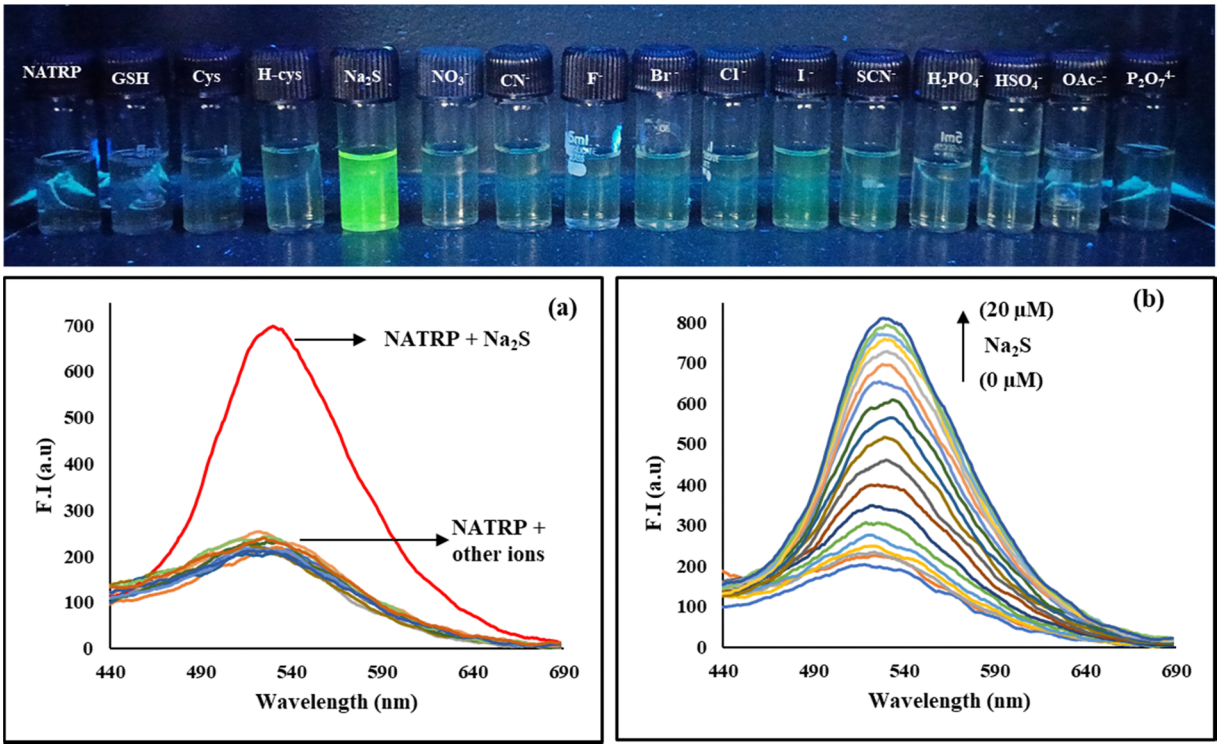

Fig. 5 Emission spectra of **NATRP** (20 μM) in a $CH_3CN : H_2O$ ratio (1 : 1, [v/v], pH = 7.3); (a) in the presence of various anions and (b) upon incremental addition (0–20 μM) of S^{2-}ions; Inset: Fluorescence color change of **NATRP** after adding different anions as seen under UV light.

been achieved. Therefore, preliminary studies were performed in $CH_3CN : H_2O$ (1 : 1), and the detection of anions was examined by recording the UV-vis spectra of **NATRP** in the absence and presence of various anions (GSH, cysteine, homocysteine, S^{2-}, NO_3^-, CN^-, F^-, Br^-, Cl^-, I^-, SCN^-, $H_2PO_4^-$, HSO_4^-, OAc^-, $P_2O_7^{4-}$) (Fig. 4a). **NATRP** exhibited an intense absorption band at 371 nm; upon addition of S^{2-} ions, the absorption band of **NATRP** showed a red shift at 430 nm along with the development of light-yellow colour, visible by the naked eye (Fig. 4, inset). Whereas, no significant change in absorption band of **NATRP** was observed with the addition of other anions. These results implied that **NATRP** exhibited excellent selectivity towards S^{2-} ions than other ions. Upon progressive addition of S^{2-} ions (0–25 μM) to the solution of **NATRP**, the absorption band at 371 nm was diminished along with the development of a new band at 430 nm and an isosbestic point at 395 nm, indicating the existence of two species in equilibrium (Fig. 4b).

3.3.2 Fluorescence response of NATRP towards anions. The emission behaviour of **NATRP** towards different anions was examined using a steady-state fluorescence spectrophotometer in order to explore the sensing ability of **NATRP** in the excited state. In $CH_3CN : H_2O$ (1 : 1 v/v), upon excitation at 375 nm, the compound displayed a weak fluorescence band at 530 nm with a quantum yield (Φ_f) of 0.27; while upon addition of S^{2-} ions to the **NATRP** solution, the emission intensity enhanced dramatically, whereas no significant change in emission intensity of **NATRP** was observed upon the addition of other anions, implying the excellent selectivity of **NATRP** towards S^{2-} ions over other ions (Fig. 5a). The visible color change was accompanied by an enhancement in fluorescence intensity seen under UV light (Fig. 5, inset). Spectrofluorimetric titrations were performed to observe the progressive variation in the emission response of the **NATRP**.S^{2-} complex. The fluorescence intensity of **NATRP** was increased upon incremental addition of S^{2-} ions (0–20 μM) into the solution of **NATRP** (Fig. 5b), with a quantum yield of 0.86, indicating the reduction of azide into amine.

3.3.3 Limit of detection and quantification. The results obtained manifested that the emission intensity of **NATRP** enhanced gradually upon incremental addition of S^{2-} ions up to 20 μM (Fig. S4, ESI†). Therefore, fluorescence spectra were used to determine the limit of detection (LOD) and limit of quantification (LOQ), which were found to be 7.9 nM and 26 nM, respectively. These low detection limits and quantification values made this compound highly efficient and sensitive toward the detection of S^{2-} ions in environmental and biological samples.

3.3.4 Interference studies. In order to validate the selective sensing of **NATRP** towards sulphide ions in the presence of other ions, an interference study was conducted. Thus, to every solution of **NATRP** (20 μM), 50 equivalents (1000 μM) of S^{2-} ions and 50 equivalents of other anions such as GSH, cysteine, homocysteine, NO_3^-, CN^-, F^-, Br^-, Cl^-, I^-, SCN^-, $H_2PO_4^-$, HSO_4^-, OAc^- and $P_2O_7^{4-}$ were added and the emission response at 520 nm was recorded for each solution. The results showed no significant change in fluorescence intensity of the **NATRP**·S^{2-} complex in the presence of these anions. Furthermore, the selectivity of **NATRP** towards S^{2-} ions in the presence

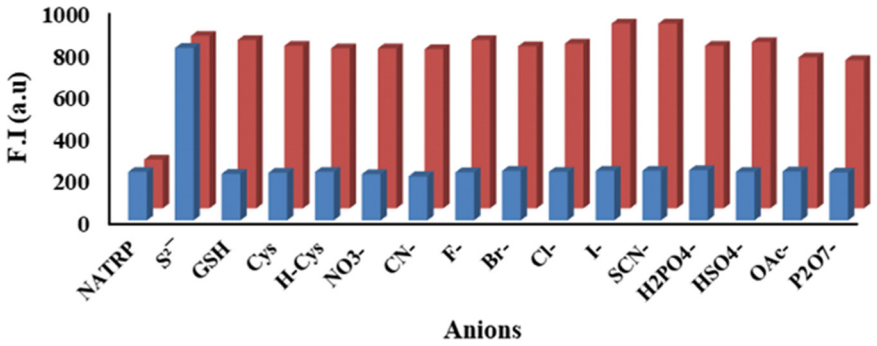

Fig. 6 Relative emission of **NATRP** (20 μM) in $CH_3CN : H_2O$ (1 : 1, v/v, pH = 7.3), (λ_{ex} = 375 nm) with various competing ions in the presence and absence of S^{2-} ions at λ_{em} = 530 nm, in which blue bars show the fluorescence intensity change of **NATRP** with various anions (50 eq.) and red bars show **NATRP** + S^{2-} with other relevant competing anions (50 eq.).

of cations and biomolecules was assessed, and no significant change in emission intensity of the **NATRP**·S^{2-} complex was recorded (Fig. S5 and S6, ESI†). This indicates that **NATRP** can selectively sense S^{2-} ions even in the presence of other potentially interfering species, demonstrating its high selectivity and suitability for practical applications in complex environments (Fig. 6).

3.3.5 Time-dependent study, pH effect and photostability of NATRP. The response time of the fluorescence probe toward analytes is an important factor for the detection of anions in real-time samples. Therefore, the time-dependent emission kinetics were conducted to determine the response time of **NATRP** towards S^{2-} ions. As shown in Fig. 7a, **NATRP** exhibited weak fluorescence at 530 nm, and no noticeable change in fluorescence intensity was observed with time in the absence of S^{2-}, whereas the addition of S^{2-} ions to **NATRP** resulted in a dramatic enhancement in emission intensity at 530 nm, which reached a plateau within 15 s. These results manifested the fast response of **NATRP**-based emission enhancement for S^{2-} ions. Thus, **NATRP** can be used to detect S^{2-} ions in real-time samples.

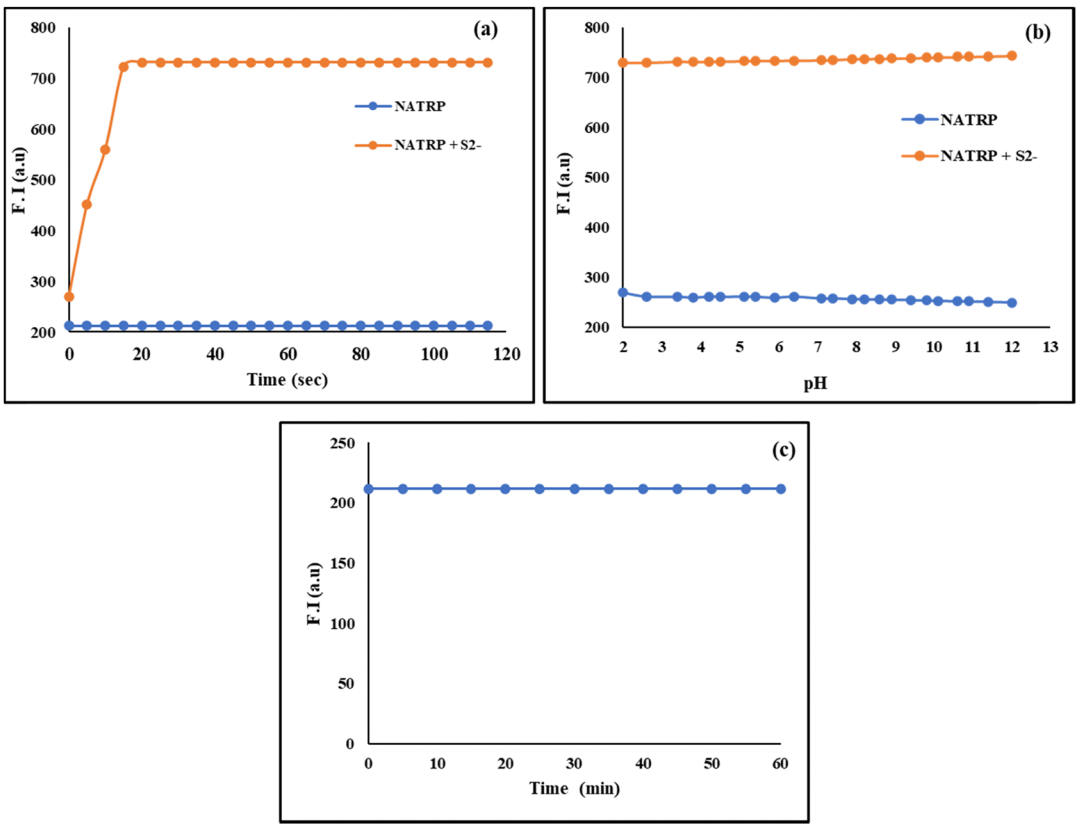

Fig. 7 (a) Time-dependent fluorescence response of **NATRP** upon addition of S^{2-} ions; (b) fluorescence intensity of **NATRP** at 530 nm obtained in the presence and absence of S^{2-} in different pH ranges in the $CH_3CN : H_2O$ (1 : 1, v/v, pH = 7.3) solvent system and (c) time-based fluorescence steady-state measurements of **NATRP** in $CH_3CN : H_2O$ (1 : 1, v/v) excited at 365 nm and monitored at 530 nm.

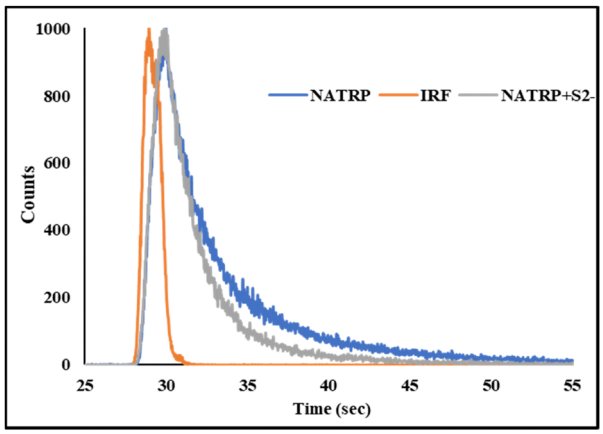

Fig. 8 Time-resolved spectra of **NATRP** ($CH_3CN : H_2O$ (1 : 1, v/v), pH = 7.3) in the absence and presence of S^{2-} ions.

Furthermore, pH titrations of **NATRP** in the absence and presence of S^{2-} ions were conducted in order to validate the sensing ability and practical applicability of **NATRP** towards S^{2-} ions in physiological conditions. The emission intensities of **NATRP** alone and in the presence of S^{2-} ions were recorded in different pH ranges (2.0–12.0), and the results are depicted in Fig. 7b. The fluorescence intensity of **NATRP** remained unchanged over a broad range of pH 2.0–12.0. The high stability of **NATRP** with varying pH ranges makes it beneficial for fast monitoring in environmental and biological samples. The reduction of azide into amine by S^{2-} ions also showed excellent stability with varying pH, ranging from 2.0–12.0. These results indicated that **NATRP** could be capable of sensing S^{2-} ions over a wide range of pH.

Time-dependent steady-state fluorescence measurements were performed on the **NATRP** probe to assess its photostability against photobleaching to ensure the experiment's accuracy and dependability. The probe in $CH_3CN : H_2O$ (1 : 1) was stimulated at 365 nm, and the emission was recorded at 530 nm. To cause photobleaching, it was then exposed to the highest level of radiation for 60 minutes. Interestingly, as illustrated in Fig. 7c, the fluorescence intensity of the **NATRP** probe remained constant even after continuous exposure, indicating the excellent photostability.

3.4 Time-correlated single photon counting (TCSPC) study

Furthermore, to get insight into the behaviour of **NATRP** towards S^{2-} ions at 375 nm, a time-correlated single photon counting experiment was performed. **NATRP** and its complex with S^{2-} ions are best fitted in bi-exponential mode, implying the existence of two different decay components (Fig. 8). For **NATRP** alone, the decay components exhibited lifetime values of 1.66 ns and 6.46 ns with a population of 72% and 28%, respectively. The average lifetime of **NATRP** was found to be 2.98 ns. Upon the addition of S^{2-} to the solution of **NATRP**, two decay components were observed with lifetimes of 1.64 ns and 4.97 ns with populations of 87% and 13%, respectively. The average lifetime was calculated to be 2.05 ns, indicating the existence of a non-radiative pathway decay (Table 2). The decrease in decay time may also be due to the reduction of azide into an amine group.

Table 2 Fluorescence lifetime measurements of **NATRP** in the absence and presence of S^{2-} ions

	τ_1 (ns)	τ_2 (ns)	α_1	α_2	τ_{av} (ns)	χ^2
NATRP	1.66	6.46	0.72	0.28	2.98	1.10
NATRP + S^{2-}	1.64	4.97	0.87	0.13	2.05	1.10

3.5 Sensing mechanism with ^{1}H NMR, HRMS and FTIR

Furthermore, to investigate the binding mechanism of S^{2-} ions with **NATRP** and the reduction of azide into an amine group, we performed ^{1}H NMR titrations and HRMS analysis. The ^{1}H NMR titrations of **NATRP** were performed in CD_3CN both in the absence and presence of S^{2-} ions. The ^{1}H NMR spectrum of **NATRP** exhibited 10 aromatic protons in the region of 8.51–6.95 ppm. Upon the addition of 0.2 equivalents of S^{2-} ions, upfield shifts in naphthalimide protons were observed; the protons at 8.51 ppm (H_e), 8.46 ppm (H_b) and 8.38 ppm (H_c) were shifted upfield to 8.42 ppm (H_e), 8.21 ppm (H_b) and 8.33 ppm (H_c), respectively (Fig. 9a). Moreover, the proton (H_d) resonating at 7.75 ppm showed a slight upfield shift to 7.59 ppm, while the proton resonating at 7.54 ppm (H_a) showed a dramatic upfield shift to 6.38 ppm due to the reduction of the azide group into an amine in the presence of S^{2-} ions. A transition state was also observed upon the addition of 0.2 eq. and 0.4 eq. S^{2-} ions to the solution of NATRP, which clearly indicated the conversion of the azide group to an amine group and the presence of an azide form and amine form in the same solution. Furthermore, the complete reduction of the azide form into an amine was observed upon addition of 1.0 eq. of S^{2-} ions, and the significant shifting in peaks of naphthalimide protons was observed, indicating the change in the electron density around the naphthalimide protons with reduction of the azide. Significant upfield shifting of H_a and H_b protons was observed, implying the complete reduction of the azide group into an amine.

To corroborate the NMR findings, HRMS analysis of **NATRP** in the presence of sulphide ions was performed (Fig. S7, ESI†), which exhibited an *m*/*z* peak at 356.1396 a.m.u corresponding to the reduction of the azide group into an amine group (**NATRP**-N_3 to **NATRP**-NH_2) and *m*/*z* + Na peak at 378.1216 corresponding to **NATRP**-NH_2 + Na^+. These results, obtained from both ^{1}H NMR titration and HRMS analysis, conclusively confirm the reduction of the azide group into an amine group in the presence of sulfide ions (Fig. 9b).

To further confirm the conversion of the azide group into an amine group in the presence of sulphide ions, we have recorded the FTIR spectrum of **NATRP** alone and in the presence of S^{2-} ion. A characteristic peak of the azide group in the region 2100–2150 cm^{-1} was seen in the IR spectrum of **NATRP** alone (Fig. 9c). This peak was diminished in the presence of S^{2-} ions, and a new peak in the region of 3300–3500 cm^{-1} was seen, which is characteristic of NH_2. Hence, the results obtained from FTIR studies further confirmed the conversion of the azide group into an amine in the presence of sulphide ions,

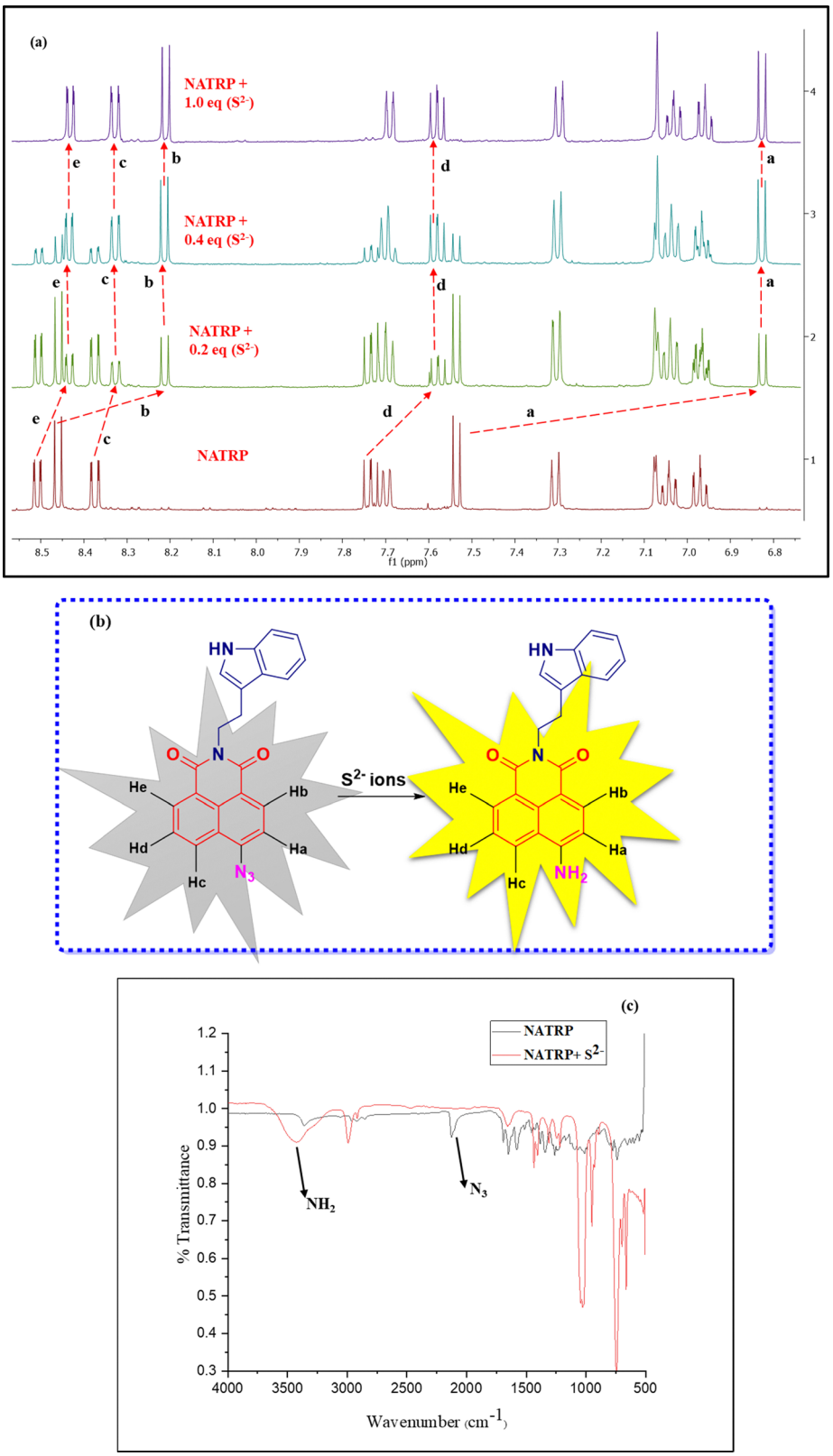

Fig. 9 (a) ^{1}H NMR titrations of **NATRP** in CD_3CN at room temperature over the incremental addition of S^{2-}; (b) proposed emission response mechanism of **NATRP**-N_3 to **NATRP**-NH_2 and (c) FTIR spectrum of **NATRP** alone and in the presence of S^{2-} ions.

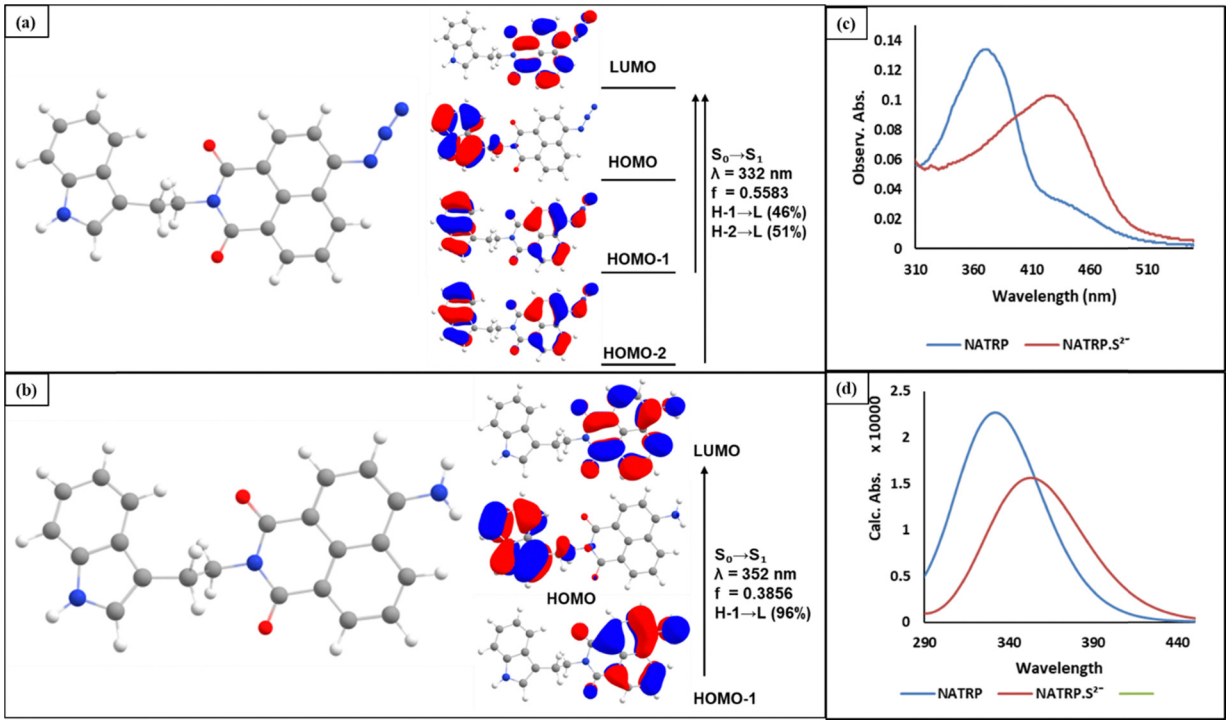

Fig. 10 Optimized structure and contributing molecular orbitals for the first excitation of (a) **NATRP** and (b) the reduced form of **NATRP**. Comparison of the observed changes through (c) observed absorption and (d) calculated excitation spectra of **NATRP** towards Na_2S.

and the results were in accordance with NMR and HRMS findings.

3.6 Computational studies

As discussed above, we have optimized compound **NATRP** in the ground state (S_0) at ωB97XD/6-311g(d) with no imaginary frequency, and three low-lying vertical excitations were calculated at the same level of theory to investigate the source of absorption spectra. For $S_0 \rightarrow S_1$, excitation determined the orbital transition contribution from the HOMO−2 → LUMO and HOMO−1 → LUMO of 51% and 46%, respectively with an oscillation strength of 0.5583 at 332 nm for **NATRP**, which is near to the experimental absorption peak at 366 nm. Additionally, for $S_0 \rightarrow S_2$ and $S_0 \rightarrow S_3$, excitations were determined at 286 nm and 285 nm with oscillation strengths of 0.0191 and 0.0004, respectively. We have only taken into consideration $S_0 \rightarrow S_1$ excitation for study because the second and the third excitations have weak oscillation strengths. The electron density analysis showed that HOMO−1 and HOMO−2 have a distribution over the molecule except for the linker ethyl unit, while the LUMO has a distribution over the naphthalimide-linked azide unit. This shift in density signified the intramolecular charge transfer from indole to the naphthalimide unit (Fig. 10a and b).

Additionally, geometry optimization was done for **NATRP**'s reduced form, and three low-lying vertical excitations that correspond to the ground state were calculated. For the reduced form of **NATRP**, the $S_0 \rightarrow S_1$ excitation determined the orbital transition contribution from HOMO−1 → LUMO of 96% with an oscillation strength of 0.3856 at 352 nm. Furthermore, oscillation strengths of 0.0002 and 0.0003 were found for the $S_0 \rightarrow S_2$ and $S_0 \rightarrow S_3$ excitations at 286 nm and 266 nm, respectively. $S_0 \rightarrow S_1$ exhibited the strongest and most notable oscillation; hence, it was further examined. According to electron density analysis, HOMO−1 and LUMO were distributed over the naphthalimide unit and indicated $\pi \rightarrow \pi^*$ transition. However, the red shift in the absorption spectra, as observed in the experiment, was mimicked through a computational approach signifying the origin of the alteration of the absorption spectra (Fig. 10c and d).

3.7 Practical applications for the detection of S^{2-} ions

3.7.1 Detection of S^{2-} ions in water and serum samples. The practical applicability of **NATRP** was examined by determining S^{2-} ions quantitatively in environmental samples. The detection of specific analytes in real samples is a difficult task due to the presence of several interfering agents in a real field. Therefore, the presence of S^{2-} ions in various water samples collected from different sources was determined by **NATRP**, as sulphide ions are released from various industrial sectors in water bodies, leading to contamination of water. Three samples were collected from various sources including (a) the Ganga river, (b) tap water from an academic laboratory, and (c) the Ghaggar river. These samples were spiked with known concentrations of S^{2-} ions (10, 20, 30, and 40 μM) externally by the standard addition method. These water samples were treated with 20 μM of **NATRP** in $CH_3CN:H_2O$ (1 : 1 v/v), and the fluorescence intensities were recorded at 530 nm (Fig. S8, ESI†). As shown in Table 3, the compound can successfully determine

Table 3 Determination of S^{2-} ions in water samples

	Spiked amount (μM)	Observed amount (μM)	Recovery (%)	RSD (%)
Ganga river	10	10.7	107	0.34
	20	22.1	110.5	0.56
	30	31.3	104.3	0.39
	40	42.6	106.5	0.48
Tap water	10	10.2	102	0.60
	20	21.6	107	0.75
	30	32.4	108	0.52
	40	41.9	104.7	0.38
Ghaggar river	10	11.7	117	0.69
	20	21.5	107.5	0.75
	30	32.8	109.3	0.49
	40	39.9	99.7	0.42

RSD: relative standard deviation.

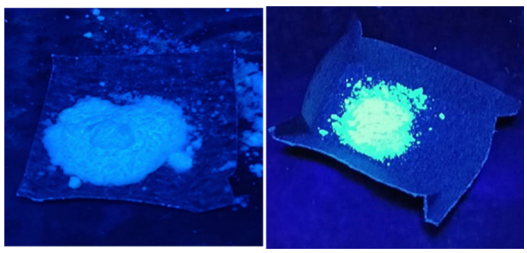

Fig. 11 Solid state detection of S^{2-} ions under UV light.

the sulphide ions in water samples, thus assisting the practical application of **NATRP**. The same studies were also performed for the detection of S^{2-} ions in serum samples with a recovery rate >98%, In addition to this, the stability of the probe in serum medium was determined, and the results implied that the fluorescence intensity of **NATRP** was relatively stable in serum medium (Table S4 and Fig. S9, ESI†).

3.7.2 Detection of S^{2-} ions in the solid phase. Furthermore, the practical applicability of **NATRP** was assessed by exploring its ability to detect the S^{2-} ions in the solid state. In the presence of S^{2-} ions, solid-state emission properties of **NATRP** were explored. The **NATRP** is non-fluorescent, as seen under a UV lamp but in the presence of S^{2-} ions (in solid state), it displayed bright greenish yellow emission (Fig. 11). Furthermore, we explored the affinity of **NATRP** towards S^{2-} in bulk samples. The addition of solid S^{2-} ions over solid **NATRP** displayed greenish yellow emission on mild mixing for 3 min under a UV lamp. These results indicated that S^{2-} ions can be detected in the solid phase too.

3.7.3 Live cell imaging. Fluorescence microscopy was employed to perform cell imaging experiments in *S. aureus* bacterial cells. As shown in Fig. 12, the cells did not exhibit any discernible fluorescence after being pre-incubated with **NATRP** for one hour, due to the weak fluorescence of the probe. However, upon subsequent treatment with a 20 μM solution of sodium sulfide (Na_2S), the cells displayed distinct green fluorescence. This result demonstrates that **NATRP** is cell-permeable and can successfully detect sulfide ions within living cells. The fluorescence activation upon exposure to Na_2S highlights the probe's potential for real-time and selective imaging of sulfide ions in biological systems.

3.7.4 Construction of a 1 to 2 decoder. In addition to the above-mentioned practical applicability of **NATRP**, we further constructed a 1 to 2 decoder by taking only one input $In_1 = S^{2-}$ and two outputs at λ_{abs} = 370 nm (OUT_1) and (OUT_2) λ_{em} = 530 nm/λ_{abs} = 430 nm. The binary digit "1" was assigned when OUT_1 $\lambda_{abs} > 0.06$ (at 370 nm), whereas "0" was allotted to the output when $\lambda_{abs} < 0.06$ (at 370 nm). Similarly, for OUT_2, "1" was assigned to the output when $\lambda_{abs} > 0.04$ (at 430 nm)/$\lambda_{em} > 150$

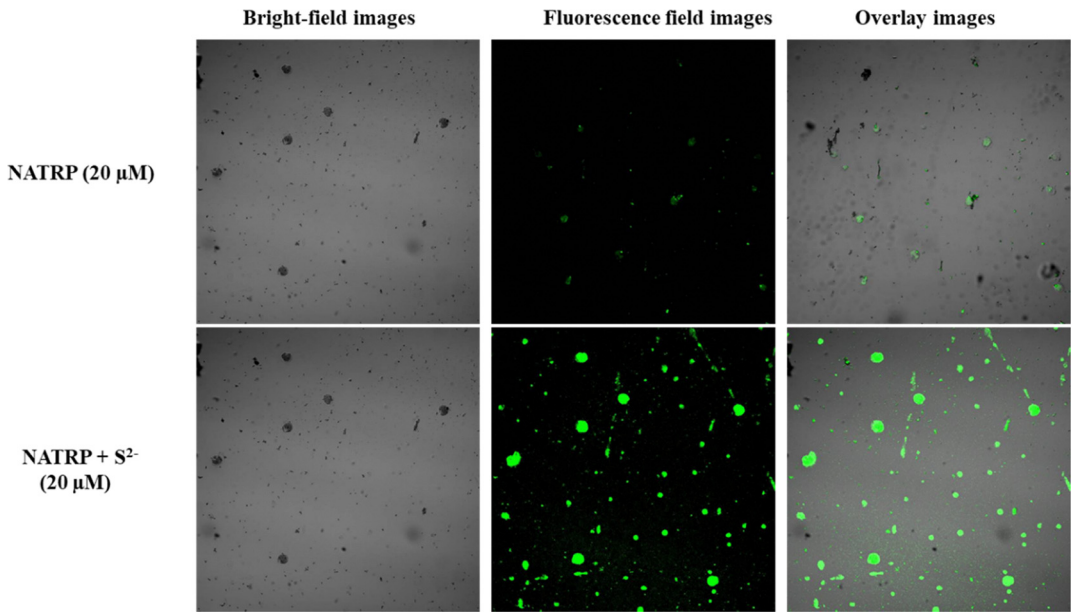

Fig. 12 Bio-imaging visualization of **NATRP** over Na_2S in live *S. aureus* cells.

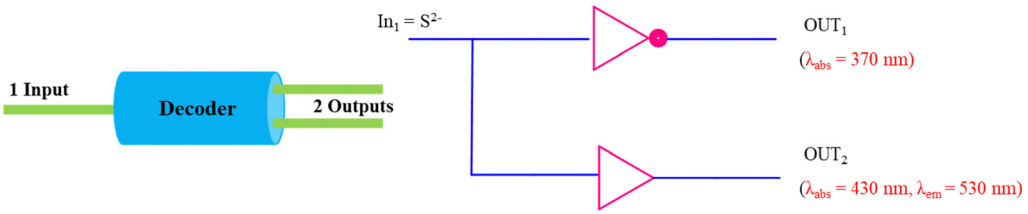

Truth Table

In_1 (S^{2-})	OUT_1 (λ_{abs} = 370 nm)	OUT_2 (λ_{abs} = 430 nm, λ_{em} = 530 nm)
0	1	0
1	0	1

Fig. 13 1-to-2 decoder with In_1 = S^{2-} and OUT_1 = 370 nm (λ_{abs}) and OUT_2 = 430 nm (λ_{abs}) or 530 nm (λ_{em}).

(at 530 nm), and "0" was given to the output when $\lambda_{abs} < 0.04$ (at 430 nm)/$\lambda_{em} < 150$ (at 530 nm). These values of "1" and "0" were allotted according to the criteria prescribed above. In the absence of In_1, OUT_1 was in the on-state, having a value of "1", and was in the off-state at OUT_2 with a value of "0". In the presence of In_1, the system was reversed where OUT_1 was in the off-state with value = 0, and OUT_2 was in the on-state with value = 1. Hence, the data of the truth table revealed that OUT_1 and OUT_2 mimicked the "NOT" and "YES" gates, respectively (Fig. 13).

4. Conclusion

In the present work, we have successfully designed and synthesized a naphthalimide-based "turn-on" fluorescent **NATRP** sensor for precise, selective, and highly sensitive detection of S^{2-} ions in $CH_3CN:H_2O$ medium (1 : 1). The **NATRP** displayed excellent selectivity and sensitivity towards S^{2-} ions with an LOD value of 7.9 nM and limit of quantification of 26 nM. The compound exhibited aggregation-induced emission quenching properties, and in the presence of S^{2-} ions, disaggregation along with enhanced fluorescence was observed. The response time of **NATRP** towards S^{2-} ions was recorded to be less than 15 s. It displayed excellent pH stability, indicating that **NATRP** can detect sulfide ions over a wide range of pH. NMR titrations and HRMS results confirmed the reduction of azide into an amine group in the presence of S^{2-} ions. Interference studies were also performed with other competitive metal ions, and compound **NATRP** can selectively detect S^{2-} ions in the presence of other ions. Furthermore, the experimental outcomes are further endorsed by computational calculation, where the observed redshift in the presence of S^{2-} ions was replicated through DFT/TD-DFT calculations. Furthermore, 1-to-2 decoder memory devices were constructed by considering the UV-visible and fluorescence results. Furthermore, the compound demonstrates the ability to detect S^{2-} ions in a variety of real samples, including water, serum, and solid samples, in addition to its efficacy in live-cell imaging of bacterial cells. This versatility highlights its potential for practical applications in environmental monitoring, clinical diagnostics, and biological research.

Data availability

The data supporting this article have been included as part of the ESI.†

Conflicts of interest

The authors declare no competing financial interest.

Acknowledgements

KP thanks SERB, New Delhi (CRG/2023/004080), and CEEMS (Project No. TIET/CEEMS/Regular/2021/018), VT-India, for providing funds. SAI labs, Acal lab and TIET for NMR and DST-FIST (SR/FST/CS-II/2018/69) for HRMS analysis are also acknowledged. We would also like to thanks Central University of Punjab for Confocal Laser. SG thanks to CEEMS-TIET/VT/8365 for providing the fellowship.

References

1 J. Wu, C. Chan, J. Li, Y. Shi, Z. Xue and L. Zhao, A BODIPY-Based Fluorescent Chemosensor with 2, 6-Substitution for Visual and Highly Selective Detection of S2–, *Spectrochim. Acta, Part A*, 2023, **297**, 122741.
2 J. Fan, E. Wu, J. Dong, R. Zhu, M. Li, J. Gao, H. Han and L. Ding, A Minimalist Ratiometric Fluorescent Sensor Based on Non-Covalent Ternary Platform for Sensing H_2S in Aqueous Solution and Serum, *Colloids Surf., A*, 2021, **616**, 126299.
3 C. Zhang, Y. Liang, W. Du, M. Kuang, Z. Meng, S. Gong, Z. Wang and S. Wang, A Novel BODIPY-Based Colorimetric Turn-on NIR Fluorescent Probe for Sensitive and Visual Detection of H_2S in Food Samples with Smartphone Platform, *J. Food Compos. Anal.*, 2024, **134**, 106518.
4 G. Lu, L. Duan, S. Meng, P. Cai, S. Ding and X. Wang, Development of a Colorimetric and Turn-on Fluorescent Probe with Large Stokes Shift for H_2S Detection and Its Multiple Applications in Environmental, Food Analysis and Biological Imaging, *Dyes Pigm.*, 2023, **220**, 111687.

5 G. Asaithambi and V. Periasamy, Hydrogen Sulfide Detection by ESIPT Based Fluorescent Sensor: Potential in Living Cells Imaging, *J. Photochem. Photobiol., A*, 2019, **369**, 97–105.
6 D. Jothi and S. K. Iyer, A Highly Sensitive Naphthalimide Based Fluorescent "Turn-on" Sensor for H_2S and Its Bio-Imaging Applications, *J. Photochem. Photobiol., A*, 2022, **427**, 113802.
7 W. Lang, J. M. Qin and Q. Y. Cao, A Novel Polymer-Based Probe for Fluorescently Ratiometric Sensing of Hydrogen Sulfide with Multiple Applications, *Anal. Chim. Acta*, 2024, **1286**, 342051.
8 Y. Mao, Q. Yu, T. Ye, M. Xi, W. Lai, Z. Chen, K. Chen, L. Li, H. Liu and J. Wang, New Rhodamine-Based Sensor for High-Sensitivity Fluorescence Tracking of Cys and Simultaneously Colorimetric Detection of H_2S, *Spectrochim. Acta, Part A*, 2024, **306**, 123589.
9 P. Sarkar, D. Das, S. Sutradhar and B. N. Ghosh, Selective Sensing of Sulphide Ion by a Simple Mercury (II) Complex of an Amino-Substituted Terpyridine in Aqueous Solution, *J. Mol. Struct.*, 2024, **1301**, 137392.
10 J. Zheng, H. L. Noh, H. W. Chun, B. M. Oh, J. Lee, S. K. Choi, E. Kim, D. Jung, W. S. Lee and J. H. Kim, Highly Sensitive, Selective, and Rapid Response Colorimetric Chemosensor for Naked Eye Detection of Hydrogen Sulfide Gas under Versatile Conditions: Solution, Thin-Film, and Wearable Fabric, *Sens. Actuators, B*, 2021, **341**, 130013.
11 V. Kavitha, P. Viswanathamurthi, J. Haribabu and C. Echeverria, An Active ESIPT Based Molecular Sensor Aided with Sulfonate Ester Moiety to Track the Presence of H_2S Analyte in Realistic Samples and HeLa Cells, *Microchem. J.*, 2023, **188**, 108484.
12 W. T. Guo, Y. F. Ding, X. Li, L. Tong, L. Dou and W. K. Dong, Highly Efficient and Selective Detection of Sulfur Ions and Picric Acid through Salamo-Cd(II) Coordination Polymer Chemosensor, *Inorg. Chim. Acta*, 2023, **557**, 121704.
13 C. Wang, Y. Gui, M. Wu, T. Wu, H. Wang, W. Gao, J. Zheng, N. Zhao, Y. Zhang, X. Shu and J. Shang, Design and Characterization of a Near-Infrared Fluorescent Probe SCN for Selective Detection of Hydrogen Sulfide (H_2S) in Living Systems and Food Samples, *J. Mol. Liq.*, 2024, **410**, 125522.
14 L. Liao, D. Guo, X. Luo, L. Meng and F. Wu, Facile Fabrication of Iron Porphyrin-Based Porous Organic Polymer with Excellent Oxidase-like Activity for Colorimetric Detection of Sulfide, *Colloids Surf., A*, 2022, **651**, 129727.
15 X. Yue, J. Wang, J. Han and B. Wang, A dual-ratiometric fluorescent probe for individual and continuous detection of H_2S and HClO in living cells, *Chem. Commun.*, 2020, **56**, 2849–2852.
16 Z. Guo, S. Park, J. Yoon and I. Shin, Recent Progress in the Development of Near-Infrared Fluorescent Probes for Bioimaging Applications, *Chem. Soc. Rev.*, 2014, **43**, 16–29.
17 X. Xiao, Y. Shen, X. Zhou, B. Sun, Y. Wang and J. Cao, Innovative Nanotechnology-Driven Fluorescence Assays for Reporting Hydrogen Sulfide in Food-Related Matrices, *Coord. Chem. Rev.*, 2023, **480**, 215012.
18 D. P. Li, J. F. Zhang, J. Cui, X. F. Ma, J. T. Liu, J. Y. Miao and B. X. Zhao, A Ratiometric Fluorescent Probe for Fast Detection of Hydrogen Sulfide and Recognition of Biological Thiols, *Sens. Actuators, B*, 2016, **234**, 231–238.
19 Z. Ju, Y. Zhang and L. Kong, A Highly Selective Fluorescent Probe for Hydrogen Sulfide and Its Application in Living Cell, *J. Fluoresc.*, 2025, **35**, 1163–1169.
20 R. Kaushik, A. Ghosh and D. Amilan Jose, Recent Progress in Hydrogen Sulphide (H_2S) Sensors by Metal Displacement Approach, *Coord. Chem. Rev.*, 2017, **347**, 141–157.
21 L. Wang, W. Yang, Y. Song and Y. Hu, Novel Turn-on Fluorescence Sensor for Detection and Imaging of Endogenous H_2S Induced by Sodium Nitroprusside, *Spectrochim. Acta, Part A*, 2020, **243**, 118775.
22 Y. M. Tian, S. S. Liu, W. N. Wu, X. L. Zhao, Y. Wang, Y. C. Fan, Z. H. Xu and T. D. James, A Mitochondria-Targeting Fluorescent Probe for the Dual-Emission Fluorescence-Enhanced Detection of Hydrogen Sulfide and Turn-on Detection of Hydrazine, *Sens. Actuators, B*, 2024, **409**, 135496.
23 H. W. Chun, J. Zheng, E. H. Lee, B. M. Oh, C. B. Lee, J. S. Min, E. Kim, E. Kim, W. Lee and J. H. Kim, Pure-Water-Soluble Colorimetric Chemosensors for Highly Sensitive and Rapid Detection of Hydrogen Sulfide: Applications to Evaluation of on-Site Water Quality and Real-Time Gas Sensors, *Sens. Actuators, B*, 2024, **402**, 134989.